GDCh Research Article Angewandte International Edition Chemie www.angewandte.org

Check for updates

How to cite: *Angew. Chem. Int. Ed.* **2025**, *64*, e202509156
doi.org/10.1002/anie.202509156

Supramolecular Chemistry Hot Paper

Tailoring Tubular Supramolecular Polymers with Polar Lumens to Host Hydrophilic Dye Molecules

Irene Sancho-Casado, Fátima Aparicio, Marina González-Sánchez, Raquel Chamorro, Víctor Vega-Mayoral, Juan Cabanillas-González, and David González-Rodríguez**

Abstract: Supramolecular polymers are living an intense research period in which new synthetic strategies, unusual morphologies, and diverse promising applications are being explored. We contribute here to this field with the development of a unique class of supramolecular polymers that are able to selectively encapsulate guest molecules within their lumen. This is achieved through a rational design of the monomer units, which self-assemble in amphiphilic cyclic entities that then stack into lipophilic tubular architectures that contain a polar pore. These tailored assemblies are able to host hydrophilic dye molecules that are complementary in size and chemical affinity for the pore coating. Dye extraction is characterized by: (1) the emergence of the dye absorption and emission features in solution, (2) a red shift of the absorption and emission maxima, caused by a confined environment of high viscosity, and (3) an energy transfer process from the monomer at the tube's walls to the included dye guest, which was characterized by photoluminescence (PL), excitation, and transient absorption measurements. When different dyes are co-encapsulated, the tubular supramolecular polymer provides a unidimensional confined chiral environment to promote sequential energy transfer processes between them.

Introduction

As an emerging class of dynamic materials, research on supramolecular polymers is living a formidable impulse.[1] Novel concepts and tools have been introduced in the last years, like kinetically controlled[2–4] and fuel-driven polymerizations,[5,6] and unprecedented degrees of structural or dynamic control have been accomplished. Moreover, the ability of supramolecular polymers to undergo reversible changes in structure and properties in response to diverse external stimuli renders them idoneous candidates for widespread applications.[7,8] Polymer backbones able to dynamically degrade and reform constitute the basis of responsive adhesives, cross-linked networks with self-healing abilities, and shape-memory materials.[9] Semiconducting π-conjugated molecules arranged in 1D stacks can display long-range charge and exciton transport, as well as unusual electrochromic and photoluminescent features, while noncovalent block copolymers have been proposed as molecular *p–n* heterojunctions.[10,11] On the other hand, supramolecular polymers incorporating biocompatible or bioactive fragments have been applied as biomimetic hierarchical structures, drug, protein, or nucleic acid delivery agents, as well as in tissue engineering and bioimaging.[12,13]

Other than supplying these mechanical, electronic, or biological functions, the constituent monomers can also be chemically programmed so as to sculpt the shape—i.e., spherical (micelles and vesicles), cylindrical (nanotubes), lamellar (nanosheets), etc.[14,15]—or even the topology—i.e., toroids, coils, etc.—[16,17] of the target supramolecular polymer across multiple hierarchical levels. This morphological control is generally attained from a uniform internal arrangement of the monomers along the supramolecular polymer and constitutes an additional element that can engender novel and more complex functions through the introduction of distinct nanophase separated regions. This additional level of functionality can give access to, for instance, the coaxial transport of electrons and holes, as proposed in segregated stacks of *n*- and *p*-type semiconducting molecules,[18–20] or the encapsulation and transport of specific molecules, as universally achieved by micellar assemblies containing differentiated lipophilic or hydrophilic domains.[21–23]

In this context, supramolecular polymers with a tubular shape, i.e., self-assembled nanotubes, stand out as highly

[*] I. Sancho-Casado, Dr. F. Aparicio, Dr. M. González-Sánchez, Dr. R. Chamorro, Prof. D. González-Rodríguez
Nanostructured Molecular Systems and Materials, Organic Chemistry Department, Universidad Autónoma de Madrid, Madrid 28049, Spain
E-mail: david.gonzalez.rodriguez@uam.es

Dr. F. Aparicio, Prof. D. González-Rodríguez
Institute for Advanced Research in Chemical Sciences (IAdChem), Universidad Autónoma de Madrid, Madrid 28049, Spain

Dr. V. Vega-Mayoral, Dr. J. Cabanillas-González
Madrid Institute for Advanced Studies, IMDEA Nanociencia, Ciudad Universitaria de Cantoblanco, Madrid 28049, Spain
E-mail: juan.cabanillas@imdea.org

Additional supporting information can be found online in the Supporting Information section

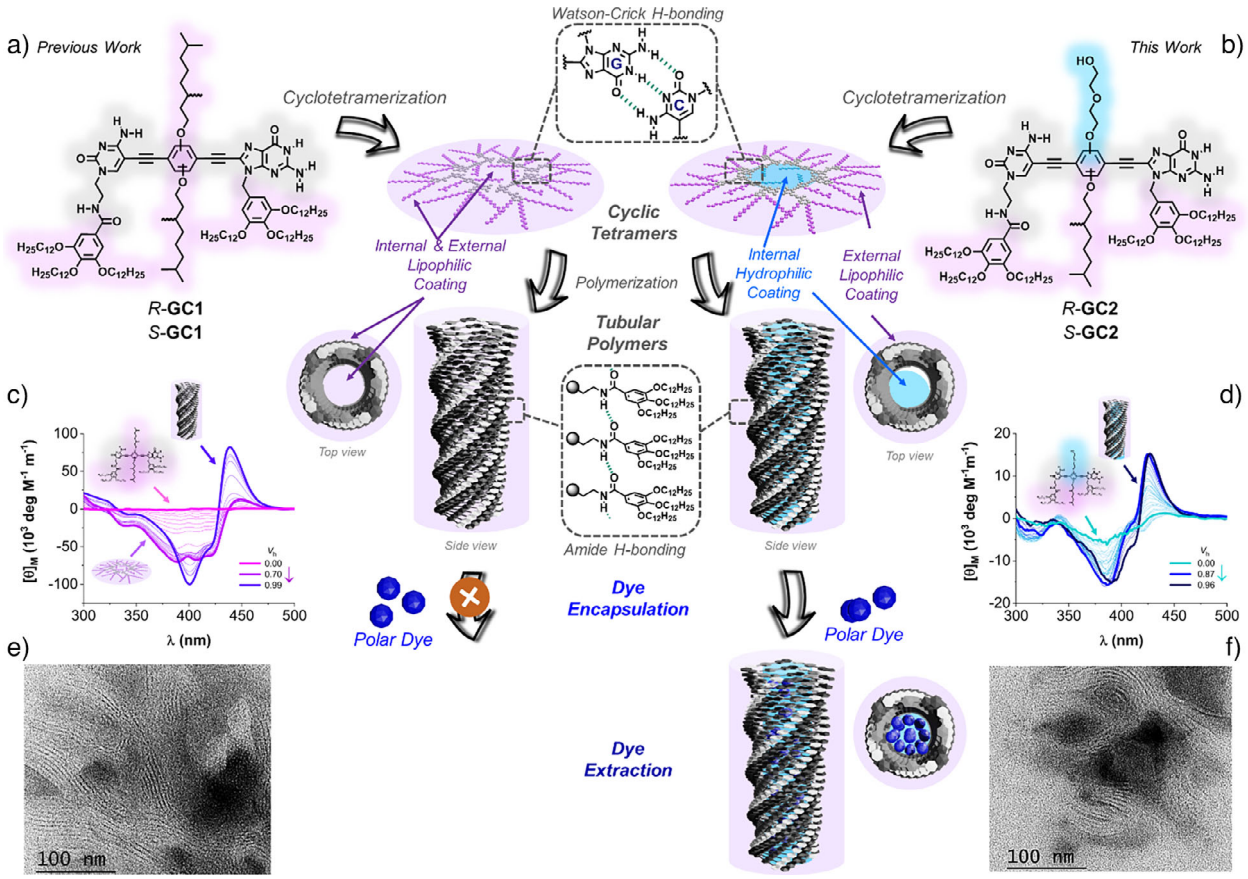

Figure 1. Self-assembly of dinucleobase monomers endowed with a) lipophilic (*R*-/*S*-**GC1**) or b) amphiphilic (*R*-/*S*-**GC2**) central blocks into nanotubes via consecutive cyclotetramerization (by Watson–Crick pairing) and polymerization (by π–π stacking and H-bonding interactions between amides) processes. In the latter, solvophobic interactions with the alkane solvent induce the formation of nanotubes with polar pores, able to extract and accommodate hydrophilic guest dyes. c), d) Supramolecular polymerization of (c) ***S*-GC1** and (d) ***S*-GC2** monitored by CD as a function of the volume fraction of heptane (V_h) in mixtures with THF. [***S*-GC1**] = $3.0{\cdot}10^{-5}$ M; [***S*-GC2**] = $5.0{\cdot}10^{-5}$ M. e), f) Representative TEM images of (e) **S-GC1** and (f) ***S*-GC2**.

appealing and versatile architectures, since they can offer structurally defined 1D inner spaces with potential applications in sensing, catalysis, biomedicine, or separation technologies.[24–28] The fascinating ability of biological tubular polymers and transmembrane channels[29,30] to host and directionally transport specific ions and other molecules across their pores represents a source of inspiration for the supramolecular chemist. Many of these tubular biosystems provide confined lumens in the attoliter scale that are chemically different from the external environment and that, as a consequence, allow access to substrate selectivity based on size and chemical affinity. A landmark example is the tobacco mosaic virus,[31] an assembly comprising 2130 copies of the same wedge-shaped protein, mainly endowed with anionic amino acids at the large site and cationic amino acids at the small site. A templated assembly process produces uniform nanotubes with positively charged pores of 4 nm in diameter, in which the negatively charged genetic material is efficiently encapsulated.

However, despite the numerous methods explored to prepare synthetic self-assembled nanotubes,[24–27] only a small fraction of studies actually exploit the chemistry within their pores.[32] One of the reasons is that the vast majority of nanotubes are made from amphiphilic molecules that afford bilayer walls, where the external and internal areas are not chemically differentiated, and thus any spontaneous encapsulation function is absent. Nanotubes with an internal coating i.e., different from the external surface, can be instead produced using inorganic templates or, in a biomimetic fashion, via the assembly of wedge-shaped bolaamphiphiles. The generated tubes have, nonetheless, pores that are typically well above 10 nm, which makes them ideal hosts for mesoscale guests like (bio)macromolecules or nanomaterials,[32] that are too large for conventional molecules. Hence, the development of supramolecular strategies toward tubular architectures with customizable pore coatings and diameters, compatible with molecular dimensions (i.e., between 1 and 10 nm), would be highly desirable to investigate novel unconventional chemical processes inside confined 1D nanospaces.

During the last years, we have developed our own approach to tubular supramolecular polymers in which two cooperative processes of different hierarchy acting in orthogonal directions are consecutively coupled (Figure 1).[33–38] Firstly, H-bonded cyclic tetramer assemblies are produced with remarkable chelate cooperativities by Watson–Crick

pairing[39,40] between guanine (G) and cytosine (C) nucleobases, installed at each end of a linear monomer.[41–43] Then, these macrocycles stack on top of each other via a nucleation-growth supramolecular polymerization process to yield helically chiral nanotubes with pore diameters that can be tailored between 1 and 5 nm, depending on the length of the central spacer connecting the bases.[44,45] We optimized this self-assembly process for *lipophilic* nanotubes,[33–35] assembled in apolar organic media through the establishment of H-bonding interactions between peripheral amide groups along the tube's axis (as in **GC1**; Figure 1a), as well as for *hydrophilic* nanotubes,[36–38] in which supramolecular polymerization in water relies on hydrophobic interactions between the macrocyclic cores. Very interestingly, in this last case, the amphiphilic design of the monomer produced cylindrical micelle-like assemblies with a hydrophilic outer coating, which enabled their solubilization in water, and a lipophilic inner pore able to host apolar substances.[36–38]

In this work we redesigned our monomers to target instead a rather unique structure in supramolecular chemistry: a lipophilic tubular polymer, and hence soluble in alkanes, endowed with a polar pore, able to selectively host molecules that are complementary in size and chemical affinity. To such end, we installed an amphiphilic central block in between the two nucleobases, bearing a lipophilic chiral tail on one side and a hydrophilic diethylene glycol chain on the other (**GC2**; Figure 1b). We reasoned that these polar groups that do not show an affinity for the external apolar media will tend to group within the tube's pore, thus affording an inner coating that would be highly polar. Such customized nanotubes should then be able to selectively extract hydrophilic (ionic) molecules that are not soluble in apolar environments but bear instead a strong chemical affinity for their internal aqueous-like tubular lumen.

Results and Discussion

Self-Assembly into Tubular Supramolecular Polymers

Thus, the amphiphilic dinucleobase compounds *S*-**GC2** and *R*-**GC2**, which differ in the chiral tail installed at the central block, were synthesized as a mixture of regioisomers, as detailed in the Supporting Information. First of all, the self-assembly of these molecules was compared to the one reported for related *S*-**GC1** and *R*-**GC1** molecules.[33–35] As shown in Figure S1, **GC2** molecules (either the *S*- or *R*-enantiomer) self-assembled in organic solvents in *c*(**GC2**)$_4$ cyclic tetramers through Watson–Crick G:C H-bonding interactions. Just like *c*(**GC1**)$_4$, the *c*(**GC2**)$_4$ cycles displayed an extraordinary stability and could not be dissociated within the 10^{-2}–10^{-5} M concentration range in apolar solvents like $CHCl_3$ or toluene. In contrast, in more H-bond-competing solvents, like THF or $CHCl_3$-DMSO mixtures, an *all-or-none* **GC2**–*c*(**GC2**)$_4$ equilibrium, in slow exchange at the NMR timescale, was observed (Figure S1A,B), which is typical of highly cooperative systems. From temperature-dependent experiments in THF at different concentrations, the enthalpy (ΔH_T), entropy (ΔS_T), equilibrium constant (K_T), and the effective molarity (*EM*) associated with the cyclotetramerization process could be calculated (Figure S1C). We determined an *EM* value of 9.2 M for the cyclotetramerization of these novel amphiphilic monomers, which is remarkably high for cyclic assemblies, in general,[46–48] but lower than the one previously calculated for lipophilic monomers having symmetric central blocks, like **GC1**. For further details, please see the Supporting Information accompanying this manuscript.[34]

On the other hand, the supramolecular polymerization of these cycles was accomplished in strongly apolar alkane solvents. A key strategy to monitor the whole self-assembly process, from the monomer to the polymeric tube, consists in slowly increasing the volume fraction of heptane (V_h) in THF solutions, from $V_h = 0$ to $V_h > 0.95$. We found that a small amount of THF is always necessary to avoid precipitation through bundling interactions between nanotubes.[33] Figure S2A compares the spectroscopic changes recorded along the polymerization of *S*-**GC1** and *S*-**GC2** by increasing V_h. Both compounds ultimately produce supramolecular polymers with similar transitions and CD spectra (Figure 1c,d), and hence identical helical chirality, despite **GC2** being actually constituted by a mixture of regioisomers with a single chiral tail. The CD spectra acquired at different V_h for *S*-**GC2** and *R*-**GC2** exhibit a mirror image relationship (Figure S2B), and the transitions recorded along the polymerization and depolymerization of these enantiomeric compounds as a function of solvent composition were identical (Figure S2C), which discards the formation of kinetic intermediates/products. Finally, TEM analysis of the **GC2** samples at high V_h, just like those of **GC1**, confirmed the formation of long tubular objects with a mean diameter that matches the rigid core of the cyclic tetramer (ca. 4 nm; Figures 1e,f, and S3). In short, the self-assembly of **GC2** is, qualitatively, virtually indistinguishable from that of **GC1**,[33–35] although some minor quantitative differences could be recorded during the cyclotetramerization and supramolecular polymerization events (see the Supporting Information for further details).

Polar Dye Encapsulation in Apolar Environments

Now, in order to explore the ability of the (**GC2**)$_n$ nanotubes to host molecules that have an affinity for the polar functional groups that are present within their lumen, we tested a series of dyes that must fulfill two conditions: (1) they should fit within the tube's cavity, of around 2.0 nm in diameter, and (2) they should be insoluble in apolar solvent mixtures at high V_h. Dye encapsulation could be monitored by optical spectroscopy techniques, namely absorption, photoluminescence (PL), and photoluminescence excitation (PLE) measurements. The outcome of these experiments for a total of 8 dyes (Rhodamine B (**RB**), Cresyl Violet (**CVio**), Methylene Blue (**MBlue**), Toluidine Blue (**TBlue**), Acid Black (**Ablack**), Cyanine 3 (a DiI analogue abbreviated hereafter as **Cy3**), Cyanine IR676 iodide (a Cy5.5 analogue, abbreviated hereafter as **Cy5**), and Cyanine HITC iodide (a Cy7 analogue, abbreviated hereafter as **Cy7**)) is presented in Figure S4, from which selected examples, using **Cy5**

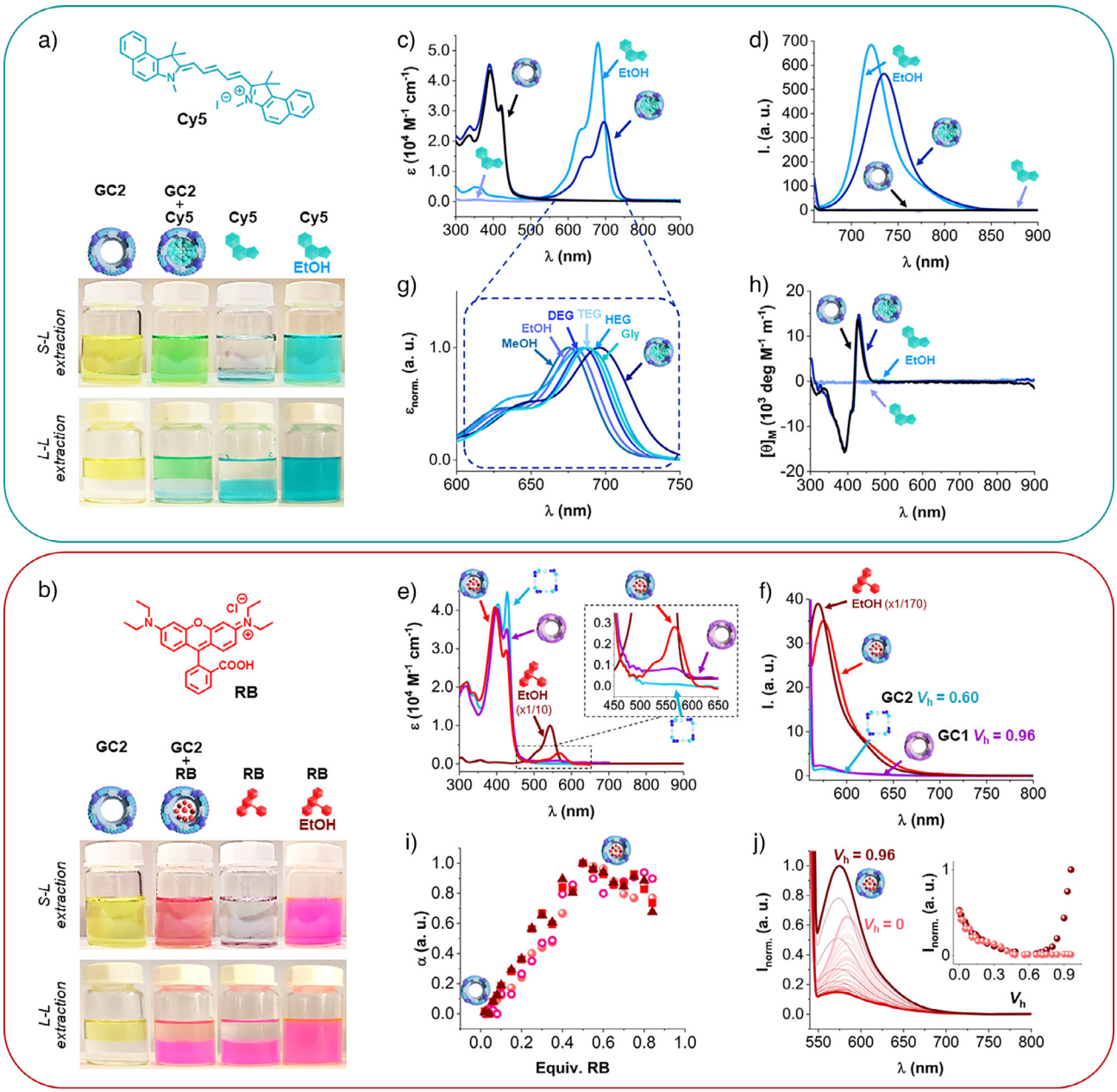

Figure 2. Extraction of a), c), d), g), h) **Cy5** and b), e), f), i), j) **RB** by *S*-**GC2** nanotubes in THF-heptane mixtures at high V_h. (a), (b) Pictures of the samples obtained after solid-liquid or liquid–liquid extraction, (c), (e) absorption, (d), (f) emission, and (h) CD spectra of: 1) *S*-**GC2**, 2) the **Cy5** or **RB** dye, and 3) their 4:1 mixture at $V_h = 0.96$, compared with: 4) the **Cy5** or **RB** dye in ethanol. In (e) and (f), the absorption and emission spectra of a 4:1 mixture of *S*-**GC2**+**RB** at $V_h = 0.60$ and of *S*-**GC1**+**RB** at $V_h = 0.96$ are also shown in blue and purple, respectively. (g) Normalized absorption spectra of **Cy5** in different solvents (methanol, ethanol, diethylene glycol (DEG), tetraethylene glycol (TEG), hexaethylene glycol (HEG) and glycerol (Gly)) and in the mixtures with *S*-**GC2** at $V_h = 0.96$. (i) Changes recorded in the absorption at 552 nm (closed circles), emission at 507 nm ($\lambda_{exc} = 380$ nm; open circles), emission at 574 nm ($\lambda_{exc} = 557$ nm; squares), and excitation spectra at 555 nm ($\lambda_{em} = 557$ nm; triangles) as increasing amounts of **RB** are mixed with *S*-**GC2** at $V_h = 0.96$. (j) Emission ($\lambda_{exc} = 525$ nm) changes occurring during the polymerization of a 4:1 *S*-**GC2**+**RB** mixture upon increasing V_h. Inset in (j) shows the magnitude of the **RB** emission intensity changes at $\lambda_{em} = 575$ nm as a function of V_h in the presence (dark red) and absence (light red) of **GC2**. In all cases, [**GC2**] = $5.0 \cdot 10^{-5}$ M.

or **RB** derivatives, are shown in Figure 2. Three primary samples were compared in a strongly apolar environment ($V_h = 0.96$): (1) the **GC2** monomer, which is assembled as helical nanotubes as discussed above, (2) the polar dye, which is totally insoluble in these conditions, and (3) a **GC2**/dye mixture in a 4:1 relative molar ratio. Moreover, the samples were prepared using two different procedures: (a) solid-liquid extraction (*S*–*L*), in which a solution of the nanotubes at $V_h = 0.96$ is added to the solid dye; and (b) liquid–liquid extraction (*L*–*L*), in which the same nanotube solution was added onto an aqueous dye solution. In both cases, the heterogeneous mixtures were stirred for 1 h and

then left to stand for over 12 h. Subsequently, the samples prepared using *S–L* extraction were centrifuged and the supernatant removed, while for the samples prepared using *L–L* extraction, the top organic phase was extracted with a pipette.

The analysis of all samples with all experimental techniques led to the same conclusion: the polar dye is only solubilized in the presence of the **GC2** amphiphilic nanotubes. This is already evidenced in the coloring of the **GC2** solutions in contact with the solid dye or the aqueous dye solution as a function of time (see Figure 2a,b for the mixtures with **Cy5** and **RB**, respectively), in comparison to **GC2** or the dye alone at $V_h = 0.96$. Pictures of **Cy5**/**RB** solutions in ethanol are also included in Figure 2a,b as a reference. Dye encapsulation was confirmed through absorption (**GC2** exhibits strong absorption bands below 450 nm, while the different dyes mostly absorb above 450 nm; Figure 2c,e) and PL measurements exciting the dye selectively (Figure 2d,f). Thus, the characteristic dye features in the red spectral region (λ_{abs} ~690 nm and λ_{em} ~750 nm for **Cy5**; λ_{abs} ~530 nm and λ_{em} ~590 nm for **RB** as shown in Figure 2c–f; see Figure S4 for the rest of the dyes) were observed when mixed with the **GC2** nanotubes, whereas the dyes on their own revealed virtually flat spectra because of their lack of solubility in this environment with high heptane content ($V_h = 0.96$).

A set of control experiments was next devised to confirm that the hydrophilic dyes were encapsulated within the polar lumen of the **GC2** nanotubes. Firstly, we carried out CD measurements (Figures 2h and S4) to verify that the nanotube helical chirality was preserved in the presence of dye, observing identical chiroptical features, both in terms of shape and intensity, to those in **GC2** samples without dye. This means that the communication between the **GC2** chiral chains is maintained along the supramolecular polymer, and hence dye intercalation in between π-stacked monomers can be ruled out. Second, to corroborate that the tubular structure is necessary to encapsulate the guests, the same kind of extraction experiments were executed under conditions in which nanotubes are not formed by reducing the heptane content down to $V_h = 0.60$. Under these conditions, **GC1** and **GC2** are only assembled as cyclic tetramers (Figure S2). Since cyanines are slightly soluble in this environment with higher THF content, **RB** was used instead. As shown in the light blue spectra in Figure 2e,f, the **GC2** samples at $V_h = 0.60$ did not exhibit the characteristic **RB** absorption and emission bands, meaning that they are unable to solubilize the dye. Third, to investigate the impact of the polar chains in the amphiphilic central block of **GC2** to enhance dye encapsulation, similar dye extraction experiments were carried out with **GC1**. As shown in the purple spectra in Figure 2e,f, **RB** absorption and emission were insignificant in the presence of the lipophilic **GC1** nanotubes, indicating that they are considerably less efficient than the amphiphilic **GC2** nanotubes in extracting polar guest molecules. Finally, in order to assess the reproducibility of these measurements and to determine the stoichiometry of the extraction process, we performed titration experiments with increasing amounts of dye and monitored the changes observed in all of these experimental techniques (Figure S5). The spectroscopic signatures attributed to dye extraction reached for all dyes (shown in Figure 2i for **RB**) a saturation above a dye/**GC2** molar ratio of 0.2–0.5, meaning that a maximum of 1–2 dye molecules can be extracted per every cyclic tetramer section in the nanotube.

We next monitored the supramolecular polymerization of **GC2** as a function of V_h in the presence of diverse dyes (Figure S6). A first objective of these experiments was to confirm that the polymerization trends with or without dye were not extremely different. A second objective was to observe the behavior of the dye when subjected to gradual solvent composition changes. Most dyes are reasonably soluble below 10^{-4} M in THF or in mixtures with heptane at very low V_h, but readily precipitate as V_h increases. So, for instance, as shown in Figure 2j, when V_h is increased in a 1:4 **RB**+**GC2** mixture, the original **RB** emission at $V_h = 0$ (partly solubilized in pure THF) first decreases down to zero, due to dye precipitation, but then, above V_h >0.8, when **GC2** starts to polymerize, **RB** emission rises again due to dye extraction within the developing nanotubes (dark red trend in the inset of Figure 2j). These results contrast with those obtained in the absence of **GC2**, where **RB** remains precipitated at high V_h (light red trend in the inset of Figure 2j).

Interestingly, the absorption and emission features of the dyes co-assembled with **GC2** at high V_h are in general red-shifted in comparison with the solutions in ethanol (see Figure 2c–f), which constitutes additional proof for their encapsulation. This gradual red shift, which closely follows the **GC2** polymerization trends, was monitored upon increasing V_h for **RB**, **Cy3**, **Cy5**, and **Cy7** dyes (Figure S6). The origin of these shifts may stem from different contributions. We discard a strong medium polarity effect, since the environment provided by the glycol chains that coat the tube pore does not differ much from solvents like ethanol, THF, or their mixtures, in which these shifts are not observed. Such shifts, consistently observed for all guest chromophores, might also come from dye aggregation or dimerization when confined within the tubular space. In fact, we observed that some dyes, like **CVio**, **MBlue,** or **TBlue**, exhibited significant emission quenching when extracted by **GC2** at high V_h (see Figure S4B–D), which may be attributed to aggregation (possibly dimerization) effects. A third reason to explain the bathochromic absorption and emission shifts resides in the viscosity of the environment, which should be very different from ethanol or THF solvents to the nanotube pore. It is known that the absorption and emission features of cyanines and related dyes are sensitive to the solvent viscosity.[49,50] In order to obtain our own experimental proof, we recorded the absorption and emission of **Cy5** in alcohols of increasing viscosity, from methanol to oligo(ethylene glycols). As shown in Figures 2g and S7, both the absorption and emission maxima of **Cy5** experience a red shift as the viscosity of the alcohol solvent increases gradually from methanol (675 and 716 nm; $\eta = 0.59$ mPa·s) to ethanol (679 and 721 nm; $\eta = 1.14$ mPa·s) to diethylene glycol (DEG; 685 and 726 nm; $\eta = 35.7$ mPa·s) to tetraethylene glycol (TEG; 687 and 727 nm; $\eta = 58.3$ mPa·s) to hexaethylene glycol (HEG; 687 and 723 nm; $\eta = \sim 80$ mPa·s) and to glycerol (Gly; 688 and 726 nm; $\eta = \sim 934$ mPa·s). Water and THF solvents also fit nicely in this trend (see Figure S7). The absorption and emission maxima exhibited by **Cy5** within the **GC2** nanotubes

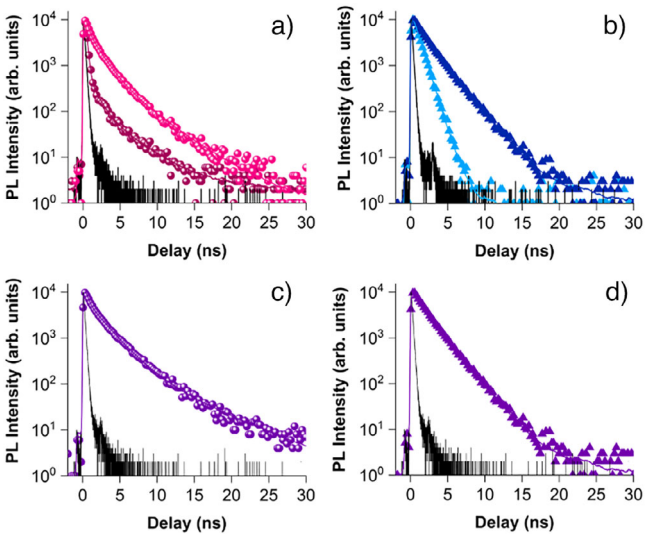

Figure 3. PL decay curves of a) **Cy3** in ethanol (magenta circles) and **GC2+Cy3** in heptane:THF (pink circles) monitored at 565 nm; b) Cy5 in ethanol (light blue triangles) and **GC2+Cy5** in heptane:THF (dark blue triangles) monitored at 720 nm; and c), d) **GC2+Cy3+Cy5** in heptane:THF monitored at c) 565 nm and at d) 720 nm. Solid lines stand for multi-exponential fits. The instrumental response function is depicted by a black line.

at $V_h = 0.96$ are 696 and 735 nm, respectively, which, by extrapolation, suggests a local environment of much higher viscosity than even the longest alcohols.

Unfortunately, and despite all efforts to try to arrive at optimized experimental conditions, no induced chirooptical effect was observed in any of the dyes extracted within the helical nanotube pore (see the collected CD spectra in Figure S4). A likely reason for this is that the guest dye is not experiencing a uniform "solvating" environment within the nanotube's pore. Please remember that the monomer is constituted by a 1:1 mixture of regioisomers and that these isomers should be distributed statistically within each cyclic tetramer section along the tube.

The inclusion of polar dye molecules, like **Cy3** and **Cy5**, within the **GC2** nanotubes leads to important changes in the dye fluorescence lifetimes. For instance, the PL decay of **Cy5** encapsulated in **GC2**'s nanotubes is bi-exponential with two decay components of 0.98 (32%) and 2.17 ns (68%) (Figure 3b), in contrast to the mono-exponential with 0.89 ns lifetime found in bare **Cy5**, in close agreement with previous reports.[51] Likewise, the fluorescence quantum yield (ϕ) of **Cy5** amounts to 0.19 and is promoted to 0.24 upon encapsulation in **GC2**'s nanotubes. The appearance of longer relaxation lifetimes in cyanines is likely related to restrictions in the rotational freedom of the dyes within the nanotube lumen. Previous studies have shown that the trans–cis photoisomerization, which plays a key role in deactivating the first singlet excited state of **Cy3** and **Cy5**, is highly sensitive to the local environment.[52,53] This is consistent with the increased viscosity proposed inside the **GC2** nanotube lumen to explain the observed bathochromic shifts. Similar differences appear when comparing **Cy3** and **Cy3** within the **CG2**'s tubes (Figure 3a), showing mono-exponential PL decay with a 0.19 ns lifetime and bi-exponential decay with 0.49 ns (54%) and 2.07 ns (46%), respectively. In line with **Cy5**, the ϕ value of **Cy3** is boosted from 0.03 to 0.12 upon **GC2** encapsulation. The complete list of PL lifetime and ϕ values are depicted in Tables S1–S4.

Energy Transfer to the Encapsulated Dyes

Solid proof for the close vicinity between the **GC2** molecules constituting the tube's walls and the guest dye stems from the observation of an efficient energy transfer between them. When mixtures of **GC2** and diverse dyes in solutions at $V_h = 0.96$ are excited at the **GC2** maximum of absorption (395 nm), where dye absorption can be neglected, the nanotube emission is drastically outbalanced by dye emission in most cases (see Figures 4b,e,h,k, and S4). Exceptions to this general observation are **Ablack**, a non-emissive dye, and **CVio**, **MBlue**, or **TBlue**, which, we believe, as mentioned above, generate non-emissive dimers/aggregates within the confined tube lumen. The occurrence of energy transfer from **GC2** to the dye molecules is further evidenced from the PLE spectra of the various dyes embedded in **GC2**, as shown in Figure 4a,d,g,j. The presence of **GC2** absorption bands upon monitoring dye emission is solid proof for energy transfer to the different dyes. Focusing on the cyanine dyes and taking **Cy5** within **GC2**'s nanotubes as an example, the PLE spectrum of **GC2+Cy5** detecting at the PL maximum of **Cy5** (Figure 4g) contains both absorption features from **GC2** and **Cy5**. On the other hand, in comparison with pristine **GC2** (Figure 4c), the 2D excitation-emission contour plot of **GC2+Cy5** (Figure 4i) reveals **GC2** resonances (red shaded areas enclosed by white square lines) in the 340–440 nm excitation range. Both observations are unambiguous proofs for a **GC2**-to-**Cy5** energy transfer process. The same evidences for energy transfer from **GC2** to the encapsulated **Cy3** dye is found in the PLE spectra (Figure 4d) and 2D excitation-emission contour plots (Figure 4f) of the **GC2+Cy3** mixture.

Energy transfer efficiencies can be evaluated from the ratio between the cyanine ϕ values measured upon **GC2** and direct cyanine photoexcitation (see Table S3).[54] Accordingly, energy transfer efficiencies of 72% and 47% were obtained for the **GC2**-to-**Cy5** and **GC2**-to-**Cy3** processes, respectively (see Section S10).

The timescales for energy transfer can be accessed with femtosecond optical transient absorption spectroscopy (TAS) measurements with 100 fs temporal resolution. The **GC2**, **GC2+Cy3**, and **GC2+Cy5** TAS contour plots obtained upon 387 nm pumping are shown in Figure 5a–c, respectively, with color bars depicting normalized changes in transmission ($\Delta T/T$). **GC2** (Figure 5a) exhibits a broad negative $\Delta T/T$ band (green shaded area) between 475 and 675 with a maximum at 573 nm ascribed to excited state absorption (ESA). The presence of this band is also seen in the TAS contour plot of the **GC2+Cy3** and **GC2+Cy5** mixtures, confirming that the energy transfer is not complete due to the limited number of cyanine molecules in the nanotube lumen. The spectral features ascribed to **Cy3** and **Cy5** manifest as red shaded areas

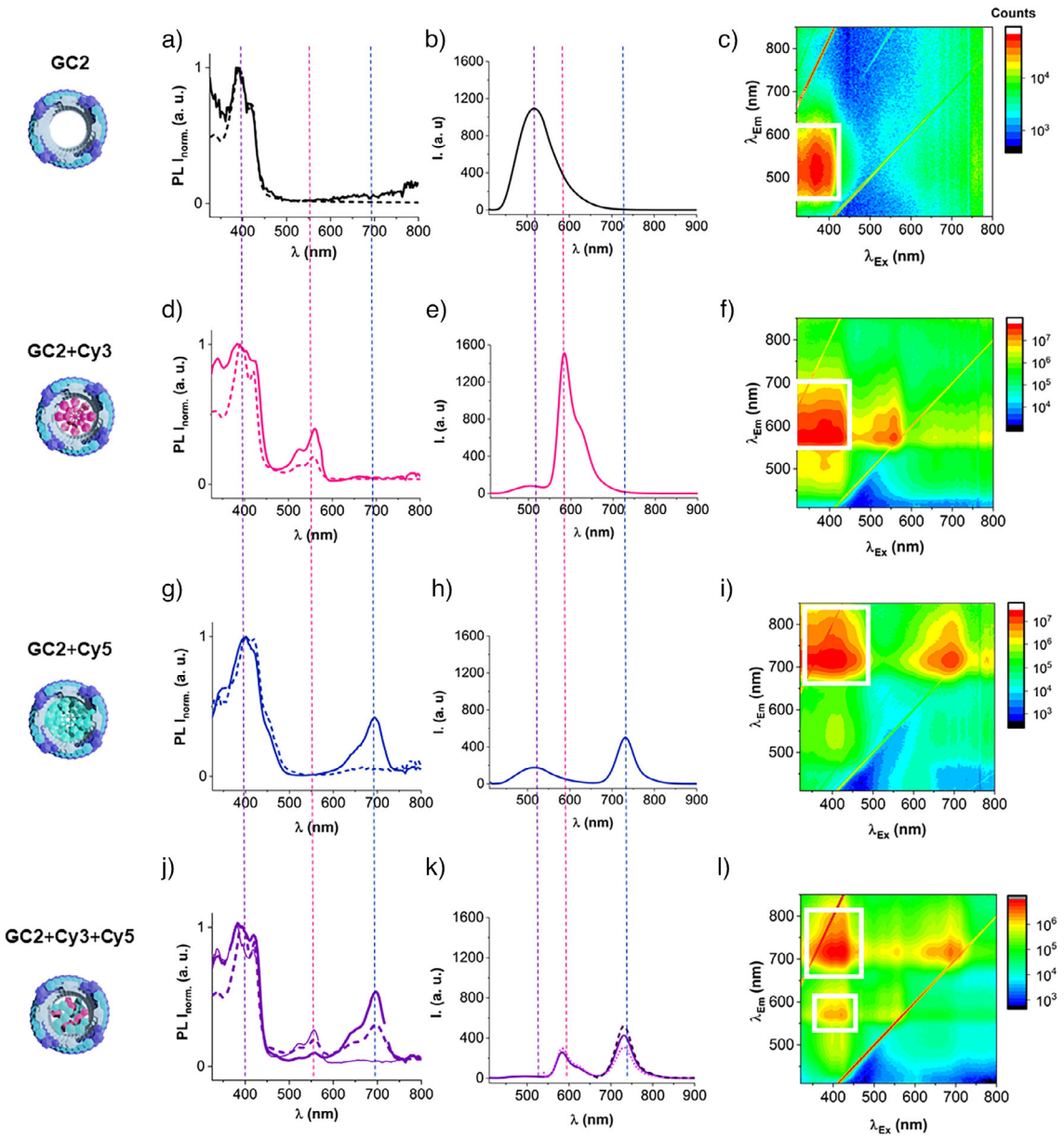

Figure 4. a), d), g), j) Absorption (dashed lines) and normalized photoluminescence-excitation spectra (PLE; solid lines; detected at: (a) 514 nm, (d) 570 nm, (g) 718 nm, and (j) 570 (thin line) or 720 nm (bold line)); b), e), h), k) Emission spectra exciting **GC2** nanotubes ($\lambda_{exc} = 395$ nm; solid lines) or (in k) **Cy3** ($\lambda_{exc} = 525$ nm; dotted line) or **Cy5** ($\lambda_{exc} = 645$ nm; dashed line); c), f), i), l) 2D Excitation-emission contour plots of: (a), (b), (c) **GC2**, (d), (e), (f) a **GC2**+**Cy3** mixture, (g), (h), (i) a **GC2**+**Cy5** mixture, and (j), (k), (l) a **GC2**+**Cy3**+**Cy5** mixture. In all cases, [**GC2**] = $5.0 \cdot 10^{-5}$ M; $V_h = 0.96$. Vertical purple, pink, and blue dotted lines indicate the absorption (in a, d, g, j) or emission (in b, e, h, k) regions of **GC2**, **Cy3**, and **Cy5**, respectively. White frames in (c), (f), (i), and (l) highlight the key spectral areas that support energy transfer. See also Figure S9 for the characterization of the cyanine samples in ethanol.

at 516 nm/553 nm (Figure 5b) and at 642 nm (Figure 5c), respectively, which stem from spectral superposition of **Cy3** and **Cy5** ground state bleach (GSB) with **GC2** ESA. The emergence of **Cy3** and **Cy5** GSB bands due to energy transfer from **GC2** is illustrated in Figure 5f,g. The ΔT/T dynamics of **GC2+Cy3** at 553 nm (magenta circles in Figure 5f) is initially dominated by **GC2** ESA (black squares in Figure 5e–h for comparison), but is gradually outbalanced by **Cy3** GSB, leading to positive ΔT/T at long delay times. Likewise, the gradual emergence of **Cy5** GSB (641 nm) in the **GC2**+**Cy5** mixtures is also visible in Figure 5g. Global analysis of the TAS kinetics (fits in Figure 5e–h and a complete analysis in Section S8 (Figure S8A–D)) provides energy transfer timescales of 1.7 ps in **GC2**+**Cy3** and 2.5 ps in **GC2**+**Cy5**.

Energy Transfer Between Co-Encapsulated Dyes

Therefore, the photophysical findings confirm the successful encapsulation of hydrophilic cyanine dyes within the polar

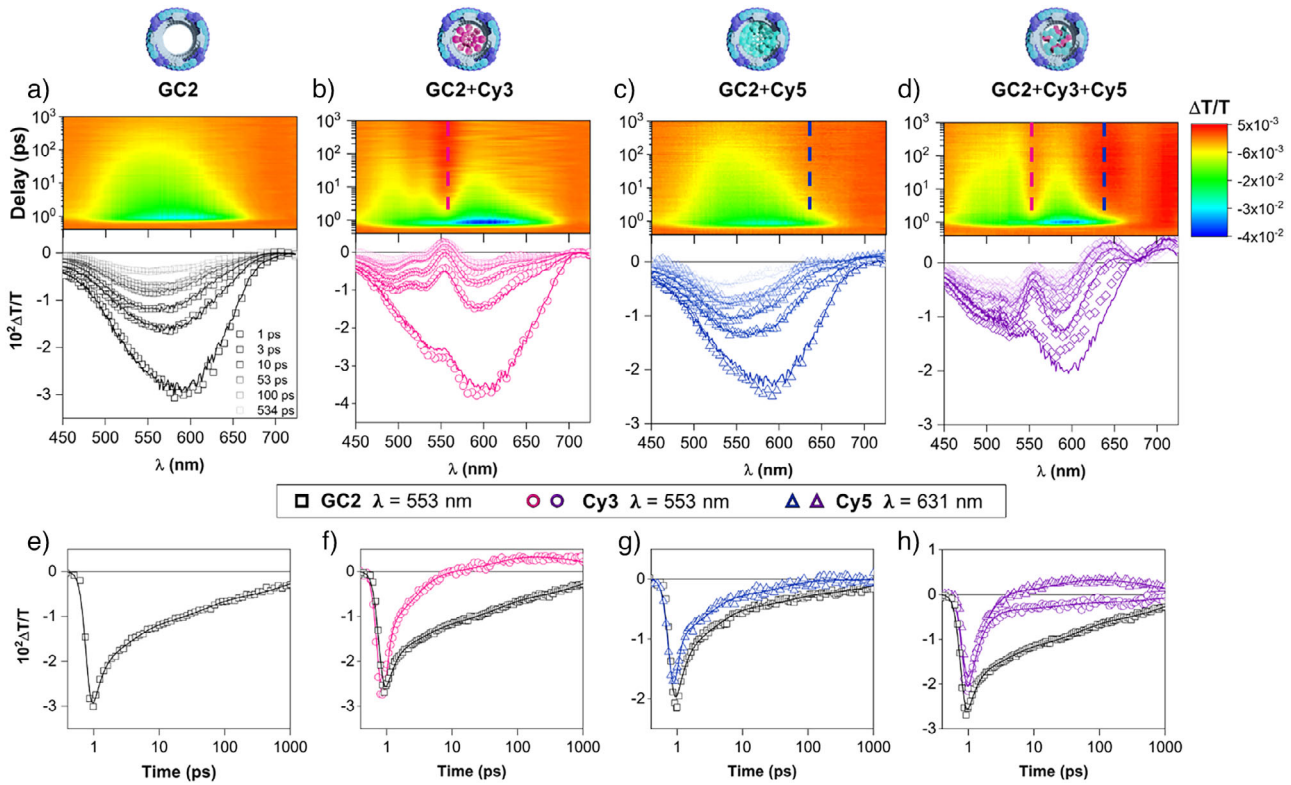

Figure 5. a)–d) TAS contour plots and TAS spectra at different time delays of (a) **GC2**, (b) a **GC2**+**Cy3** mixture, (c) a **GC2**+**Cy5** mixture, and (d) **GC2**+**Cy3**+**Cy5** mixture. The magenta and cyan dashed vertical lines in (b–d) depict the spectral positions of the **Cy3** (553 nm) and **Cy5** (631 nm) GSB bands, respectively. e)–h) TAS dynamics of (e) **GC2** monitored at 576 nm, (f) **GC2** and **GC2**+**Cy3** monitored at 553 nm, (g) **GC2** and **GC2**+**Cy5** monitored at 631 nm, and (h) **GC2** monitored at 553 nm and **GC2**+**Cy3**+**Cy5** monitored at 553 nm and 631 nm. The pump excitation was placed at 387 nm, coinciding with the maximum absorption of **GC2**. Symbols stand for the TAS experimental data, whereas lines depict fits obtained from global analysis.

lumen of the nanotubes assembled from **GC2** molecules, as well as the intimate contact between the **GC2** chromophores and the cyanine guests, manifested by a picosecond energy transfer interaction between them. Our next immediate challenge was to test the ability of these amphiphilic nanotubes to co-host two different dyes and afford a confined environment that could promote photophysical interactions between them. In view of the results obtained so far, we chose the **Cy3** and **Cy5** dye combination, since they constitute a well-known pair of donor–acceptor energy transfer chromophores.[55,56] Thus, dilute solutions of ternary mixtures of **GC2**, **Cy3**, and **Cy5** in an 8:1:1 ratio were next studied in a highly apolar environment at $V_h = 0.96$ and compared with the previously studied **GC2**+**Cy3** and **GC2**+**Cy5** binary mixtures under the same conditions (Figure S11A).

As shown in Figures 4j and S11A, the absorption spectra of the **GC2**+**Cy3**+**Cy5** combination disclosed the electronic absorption transitions of the three chromophores at ca. 400, 550, and 700 nm, respectively, which indicated their successful co-solubilization. Moreover, a comparison of the absorbance of binary and ternary mixtures suggested that cyanine extraction occurred statistically, meaning that the nanotubes did not show a measurable preference to host selectively one of the cyanine dyes. As in the case of the individual dyes, the mixture of **Cy3**+**Cy5** in the absence of **GC2**'s nanotubes was totally insoluble at $V_h = 0.96$, revealing flat absorption and emission spectra (Figure S11A).

Turning our attention to the emission features of the co-encapsulated cyanines, we again noted the same viscosity-induced red-shifts in comparison to the **Cy3**+**Cy5** samples dissolved in ethanol (Figure S11A). Moreover, the PL decay curves of **Cy3** and **Cy5** exhibited longer dynamics when both are included in the **GC2** lumen (Figure 3c,d) than they do when incorporated separately into **GC2** (Figure 3a,b), confirming that the PL properties of **Cy3** and **Cy5** in the mixtures are preserved.

Next, energy transfer events from the **GC2** chromophores in the tube walls to the included dyes, on one hand, and between co-encapsulated cyanines, on the other, were examined. Selective excitation of **GC2** in the **GC2**+**Cy3**+**Cy5** mixtures resulted in the emission spectrum shown in Figure 4k (solid line), where **GC2** fluorescence is almost completely quenched and the emission of both **Cy3** and **Cy5** dyes at ca. 580 and 730 nm is notable. When, interestingly, **Cy3** was selectively excited in the same ternary mixture (dotted line in Figure 4k), the emission of this cyanine was also significantly quenched with respect to the reference **GC2**+**Cy3** binary combination in the same conditions, and an intense **Cy5** emission at 730 nm was again recorded (see also Figure S11A). This evidence speaks of sequential

energy transfer processes between the three chromophores, which were corroborated through excitation measurements. For instance, in the PLE spectra of the **GC2**+**Cy3**+**Cy5** mixtures detected at 570 or 720 nm (thin and bold solid lines in Figure 4j, respectively), the contribution of **GC2** to **Cy3** emission, in the first case, and of both **GC2** and **Cy3** to **Cy5** emission, in the second, was clearly noted. Likewise, the 2D excitation-emission contour plot shown in Figure 4l manifests the contribution of **GC2** to the emission of both cyanines and the additional contribution of **Cy3** to **Cy5** emission. It is important to remark at this point that 1:1 **Cy3**+**Cy5** mixtures dissolved in ethanol within the same concentration range do not show any evidence of energy transfer between them (Figure S9), and absorption, emission, and excitation spectra are basically a superimposition of the individual samples (k). This substantiates the idea that the two guest dyes must be in close proximity within the confined pore nanospaces to promote secondary energy transfer processes between them. We would also like to point out that ternary mixtures combining other cyanines, like **GC2**+**Cy3**+**Cy7** (Figure S11B) and **GC2**+**Cy5**+**Cy7** (Figure S11C), were also subjected to absorption, emission, and excitation measurements, revealing similar cascades of energy transfer events between the three chromophores.

Finally, energy transfer dynamics in the **GC2**+**Cy3**+**Cy5** mixtures were studied in TAS measurements. Energy transfer from **GC2** to **Cy3**/**Cy5** takes place in about 1 ps. Notably, the TAS spectra at different delays in Figure 5d, along with the global analysis, show that, while the spectral features of **Cy3** dominate at early times, those of **Cy5** become more prominent beyond 10 ps. This gradual spectral evolution is ascribed to some **Cy3** molecules, which, being in close proximity to **Cy5**, undergo energy transfer, as already supported by the PLE measurements. According to the global analysis, the energy transfer from **Cy3** to **Cy5** would proceed in about 23 ps.

Conclusion

Research in supramolecular polymers is experiencing an intense, highly productive period in which new synthetic strategies, unusual novel morphologies, and diverse promising applications are being developed. This work intends to contribute to this current through the introduction of function in the form of selective molecular encapsulation within the tailored lumen of these unidimensional structures. In particular, we described herein the noncovalent synthesis of unprecedented tubular polymer structures that are soluble in apolar organic solvents but are endowed with pores having a polar inner coating. This is achieved by programming monomer structure with complementary G and C nucleobases at the edges and with an amphiphilic π-conjugated block in the center. The supramolecular tubular assemblies generated are able to encapsulate very efficiently polar dyes that are not soluble in the external alkane medium. However, these dyes may interact efficiently with the inner nanotube coating, potentially establishing ion-dipole, dipole–dipole and H-bonding interactions with the ethylene glycol chains and internal functional groups at the nucleobases. Dye extraction is mainly characterized by: (a) the emergence of the dye absorption and emission features in solution, (b) a red shift of the absorption and emission maxima, likely caused by a confined environment of high viscosity, and (c) an energy transfer process from the **GC2** chromophores at the tube's walls to the included dye guest. This excitation transfer process was further studied through PL quantum yield, excitation, and transient absorption measurements, which, in the case of the **Cy5** dye, revealed an energy transfer occurring within the first picoseconds after photoexcitation with an efficiency up to 72% from **GC2** to the cyanine. Furthermore, we proved that these custom-tailored nanotubes could be employed as containers for multiple cyanine dyes, which can undergo a cascade of energy transfer events as a result of their co-encapsulation within the confined pore nanospaces. An interesting question to be addressed in the future is whether these cylindrical nanosystems show strong encapsulation selectivities between polar dyes of different natures.

Acknowledgements

D.G.-R. acknowledges funding from MCIN/AEI and Next Generation EU through projects PID2020-116921GB-I00, TED2021-132602B-I00, and PID2023-148548NB-I00. F.A. is grateful to funding from project PID2020-116112RJ-I00 and grant RyC-2021–031538-I. V V.-M. acknowledges grants TED2021-131906A-100 and RYC2022-035200-I funded by Spanish Ministry of Science, Innovation and Universities (10.13039/501100011033) and support from the Regional Government of Madrid (2019-T2/IND-12737 and 2024-T1/TEC-31349). J.C.-G acknowledges the MICINN-FEDER (projects PID2021-128313OB-I00, PDC2023-145871-I00), the Regional Government of Madrid (TEC- 2024/TEC-459_SYNMOLMAT-CM), and is grateful for a Research Consolidation Grant (CNS2022-36191) from the Spanish Ministry of Science and Innovation. IMDEA Nanociencia acknowledges support from the "Severo Ochoa" Programme for Centres of Excellence in R&D of the Spanish Ministry of Science and Innovation (CEX2020-001039-S).

Conflict of Interests

The authors declare no conflict of interest.

Data Availability Statement

The data that support the findings of this study are available in the Supporting Information of this article.

Keywords: Chiral helical nanostructures · Nucleobase self-assembly · Self-assembled nanotubes · Supramolecular polymers

[1] T. Aida, E. W. Meijer, *Isr. J. Chem.* **2020**, *60*, 33–47.
[2] J. Matern, Y. Dorca, L. Sánchez, G. Fernández, *Angew. Chem. Int. Ed.* **2019**, *58*, 16730–16740.

[3] S. Dhiman, S. J. George, *Bull. Chem. Soc. Jpn.* **2018**, *91*, 687–699.
[4] M. Wehner, F. Würthner, *Nat. Rev. Chem.* **2020**, *4*, 38–53.
[5] A. Sorrenti, J. Leira-Iglesias, A. J. Markvoort, T. F. A. de Greef, T. M. Hermans, *Chem. Soc. Rev.* **2017**, *46*, 5476–5490.
[6] A. Sharko, D. Livitz, S. De Piccoli, K. J. M. Bishop, T. M. Hermans, *Chem. Rev.* **2022**, *122*, 11759–11777.
[7] T. Aida, E. W. Meijer, S. I. Stupp, *Science* **2012**, *335*, 813–817.
[8] L. Yang, X. Tan, Z. Wang, X. Zhang, *Chem. Rev.* **2015**, *115*, 7196–7239.
[9] A. D. O'Donnell, S. Salimi, L. R. Hart, T. S. Babra, B. W. Greenland, W. Hayes, *React. Funct. Polym.* **2022**, *172*, 105209.
[10] A. Jain, S. J. George, *Mater. Today* **2015**, *18*, 206–214.
[11] H. Chen, J. F. Stoddart, *Nat. Rev. Mater.* **2021**, *6*, 804–828.
[12] R. Dong, Y. Zhou, X. Huang, X. Zhu, Y. Lu, J. Shen, *Adv. Mater.* **2015**, *27*, 498–526.
[13] H. Wang, J. Mills, B. Sun, H. Cui, *Prog. Polym. Sci.* **2024**, *148*, 101769.
[14] D. Lombardo, M. A. Kiselev, S. Magazù, P. Calandra, *Adv. Condens. Matter Phys.* **2015**, *2015*, 1–22.
[15] M. Ramanathan, L. K. Shrestha, T. Mori, Q. Ji, J. P. Hill, K. Ariga, *Phys. Chem. Chem. Phys.* **2013**, *15*, 10580–10611.
[16] S. Yagai, Y. Kitamoto, S. Datta, B. Adhikari, *Acc. Chem. Res.* **2019**, *52*, 1325–1335.
[17] S. Datta, Y. Kato, S. Higashiharaguchi, K. Aratsu, A. Isobe, T. Saito, D. D. Prabhu, Y. Kitamoto, M. J. Hollamby, A. J. Smith, R. Dalgliesh, N. Mahmoudi, L. Pesce, C. Perego, G. M. Pavan, S. Yagai, *Nature* **2020**, *583*, 400–405.
[18] Y. Yamamoto, T. Fukushima, Y. Suna, N. Ishii, A. Saeki, S. Seki, S. Tagawa, M. Taniguchi, T. Kawai, T. Aida, *Science* **2006**, *314*, 1761–1764.
[19] H. Kar, S. Ghosh, *Isr. J. Chem.* **2019**, *59*, 881–891.
[20] R. De, S. K. Pal, *Chem. Commun.* **2023**, *59*, 3050–3066.
[21] R. Thipparaboina, R. B. Chavan, D. Kumar, S. Modugula, N. R. Shastri, *Colloids Surf. B* **2015**, *135*, 291–308.
[22] V. P. Torchilin, *Pharm. Res.* **2006**, *24*, 1–16.
[23] Z. Ahmad, A. Shah, M. Siddiq, H.-B. Kraatz, *RSC Adv.* **2014**, *4*, 17028–17038.
[24] M. Sun, M. Lee, *Acc. Chem. Res.* **2021**, *54*, 2959–2968.
[25] T. Shimizu, W. Ding, N. Kameta, *Chem. Rev.* **2020**, *120*, 2347–2407.
[26] R. García-Fandiño, M. Amorín, J. R. Granja, in *Supramolecular Chemistry* (Eds: P. A. Gale, J. W. Steed), Wiley, Hoboken, NJ **2012**, pp. 1–34, https://doi.org/10.1002/9780470661345.smc081.
[27] P. B. Chamorro, F. Aparicio, *Chem. Commun.* **2021**, *57*, 12712–12724.
[28] Q. Song, Z. Cheng, M. Kariuki, S. C. L. Hall, S. K. Hill, J. Y. Rho, S. Perrier, *Chem. Rev.* **2021**, *121*, 13936–13995.
[29] T. Yan, J. Liu, *Angew. Chem. Int. Ed.* **2025**, *64*, e202416200.
[30] J. M. H. Saier, *J. Membr. Biol.* **2000**, *175*, 165–180.
[31] A. N. H. Creager, *Annu. Rev. Virol.* **2022**, *9*, 39–55.
[32] T. Komatsu, *Nanoscale* **2012**, *4*, 1910–1918.
[33] V. Vázquez-González, M. J. Mayoral, R. Chamorro, M. M. R. M. Hendrix, I. K. Voets, D. González-Rodríguez, *J. Am. Chem. Soc.* **2019**, *141*, 16432–16438.
[34] V. Vazquez-Gonzalez, M. J. Mayoral, F. Aparicio, P. Martinez-Arjona, D. Gonzalez-Rodriguez, *ChemPlusChem* **2021**, *86*, 1087–1096.
[35] M. González-Sánchez, M. J. Mayoral, V. Vázquez-González, M. Paloncýová, I. Sancho-Casado, F. Aparicio, A. de Juan, G. Longhi, P. Norman, M. Linares, D. González-Rodríguez, *J. Am. Chem. Soc.* **2023**, *145*, 17805–17818.
[36] F. Aparicio, P. B. Chamorro, R. Chamorro, S. Casado, D. González-Rodríguez, *Angew. Chem. Int. Ed.* **2020**, *59*, 17091–17096.
[37] P. B. Chamorro, F. Aparicio, R. Chamorro, N. Bilbao, S. Casado, D. González-Rodríguez, *Org. Chem. Front.* **2021**, *8*, 686–696.
[38] F. Aparicio, I. Sancho-Casado, P. B. Chamorro, M. Gonzalez-Sanchez, S. Pujals, V. Vega-Mayoral, D. Gonzalez-Rodriguez, *Chem. Eur. J.* **2024**, *30*, e202402365.
[39] J. Camacho-García, C. Montoro-García, A. M. López-Pérez, N. Bilbao, S. Romero-Pérez, D. González-Rodríguez, *Org. Biomol. Chem.* **2015**, *13*, 4506–4513.
[40] A. del Prado, D. González-Rodríguez, Y.-L. Wu, *ChemistryOpen* **2020**, *9*, 409–430.
[41] S. Romero-Pérez, J. Camacho-García, C. Montoro-García, A. M. López-Pérez, A. Sanz, M. J. Mayoral, D. González-Rodríguez, *Org. Lett.* **2015**, *17*, 2664–2667.
[42] C. Montoro-García, J. Camacho-García, A. M. López-Pérez, M. J. Mayoral, N. Bilbao, D. González-Rodríguez, *Angew. Chem. Int. Ed.* **2016**, *55*, 223–227.
[43] D. Serrano-Molina, C. Montoro-García, M. J. Mayoral, A. de Juan, D. González-Rodríguez, *J. Am. Chem. Soc.* **2022**, *144*, 5450–5460.
[44] C. Montoro-García, M. J. Mayoral, R. Chamorro, D. González-Rodríguez, *Angew. Chem. Int. Ed.* **2017**, *56*, 15649–15653.
[45] M. González-Sánchez, M. J. Mayoral, F. Aparicio, V. Vázquez-González, I. Sancho-Casado, E. Anaya-Plaza, D. González-Rodríguez, *Angew. Chem. Int. Ed.* **2025**, *64*, e202413321.
[46] F. Aparicio, M. J. Mayoral, C. Montoro-García, D. González-Rodríguez, *Chem. Commun.* **2019**, *55*, 7277–7299.
[47] D. Serrano-Molina, A. de Juan, D. González-Rodríguez, *Chem. Rec.* **2021**, *21*, 480–497.
[48] P. Motloch, C. A. Hunter, in *Advances in Physical Organic Chemistry*, vol. *50* (Eds: I. H. Williams, N. H. Williams), Academic Press, Amsterdam, The Netherlands **2016**, pp. 77–118, https://doi.org/10.1016/bs.apoc.2016.07.001.
[49] F. Fan, V. A. Povedailo, I. L. Lysenko, T. P. Seviarynchyk, O. L. Sharko, I. O. Mazunin, V. V. Shmanai, *J. Fluoresc.* **2024**, *34*, 925–933.
[50] P. F. Aramendia, R. M. Negri, E. S. Roman, *J. Phys. Chem.* **1994**, *98*, 3165–3173.
[51] D. A. Helmerich, G. Beliu, S. S. Matikonda, M. J. Schnermann, M. Sauer, *Nat. Methods* **2021**, *18*, 253–257.
[52] M. E. Sanborn, B. K. Connolly, K. Gurunathan, M. Levitus, *J. Phys. Chem. B* **2007**, *111*, 11064–11074.
[53] Z. Huang, D. Ji, S. Wang, A. Xia, F. Koberling, M. Patting, R. Erdmann, *J. Phys. Chem. A* **2006**, *110*, 45–50.
[54] T. Virgili, D. G. Lidzey, D. D. C. Bradley, *Adv. Mater.* **2000**, *12*, 58–62.
[55] R. Roy, S. Hohng, T. Ha, *Nat. Methods* **2008**, *5*, 507–516.
[56] D. K. Sasmal, L. E. Pulido, S. Kasal, J. Huang, *Nanoscale* **2016**, *8*, 19928–19944.

Manuscript received: April 25, 2025
Revised manuscript received: June 20, 2025
Accepted manuscript online: July 02, 2025
Version of record online: July 14, 2025